Infrared Physics & Technology 85 (2017) 66–73

Contents lists available at ScienceDirect

Infrared Physics & Technology

journal homepage: www.elsevier.com/locate/infrared

Regular article

Spherical warm shield design for infrared imaging systems

Qijie Tian [a,b,*], Songtao Chang [a], Fengyun He [a], Zhou Li [a,b], Yanfeng Qiao [a]

[a] Changchun Institute of Optics, Fine Mechanics and Physics, Chinese Academy of Sciences, Changchun, Jilin 130033, China
[b] University of Chinese Academy of Sciences, Beijing 100049, China

HIGHLIGHTS

- The detailed theory of spherical warm shield design is introduced.
- A polished spherical warm shield is designed based on the theory above.
- The stray radiation suppression performance and the alignment error are analyzed by simulation.
- Experimental results indicate that the designed spherical warm shield can suppress stray radiation sufficiently.

ARTICLE INFO

Article history:
Received 13 March 2017
Revised 16 May 2017
Accepted 24 May 2017
Available online 25 May 2017

Keywords:
Spherical warm shield
Infrared imaging system
Stray radiation
Radiometric calibration

ABSTRACT

The F-number matching is the primary means to suppress stray radiation for infrared imaging systems. However, it is difficult to achieve exact F-number matching, owing to the restriction from detectors, or multiple F-number design. Hence, an additional shield is required to block the certain thermal radiation. Typical shield is called flat warm shield, which is flat and operates at room temperature. For flat warm shield, it cannot suppress stray radiation while achieving F-number matching. To overcome the restriction, a spherical reflective warm shield is required. First of all, the detailed theory of spherical warm shield design is developed on basis of the principle that stray radiation cannot directly reach the infrared focal plane array. According to the theory developed above, a polished spherical warm shield, whose radius is 18 mm, is designed to match an F/2 infrared detector with an F/4 infrared imaging system. Then, the performance and alignment errors of the designed spherical warm shield are analyzed by simulation. Finally, a contrast experiment between the designed spherical warm shield and two differently processed flat warm shields is performed in a chamber with controllable inside temperatures. The experimental results indicate that the designed spherical warm shield cannot only achieve F-number matching but suppress stray radiation sufficiently. Besides, it is demonstrated that the theory of spherical warm shield design developed in this paper is valid and can be employed by arbitrary infrared imaging systems.

1. Introduction

Stray radiation, known as the stray light, refers to the unwanted radiation or light that reaches the infrared focal plane array (IRFPA). Stray radiation can reduce the signal to noise ratio (SNR) of images [1,2]. There are many methods to improve the stray radiation suppression performance of an infrared imaging system. But for cryogenic infrared imaging systems, the primary means of reducing stray radiation is to take the cold stop as the aperture stop, namely the F-number matching or 100% cold shield efficiency [3,4]. When the F-number matching is achieved, which means the F-number of optics equals to the F-number of detector, only the radiation inside the field of view (FOV) can reach the IRFPA [5,6], as shown in Fig. 1. As a result, the stray radiation is suppressed sufficiently. However, it is difficult to achieve the accurate F-number matching in practical applications, due to the restriction from detectors or the requirement for multiple F-number design, etc. For example, the F-number of typical cryogenic infrared detectors is F/2 or F/4, which means in order to suppress stray radiation, the F-number of infrared imaging systems must be equivalent to F/2 or F/4. As a result, we cannot build infrared imaging systems with other F-number, such as F/8 or greater.

To achieve exact F-number matching, an additional shield is required to block certain thermal radiation, as shown in Fig. 2. Typical shield is called flat warm shield, which is flat and operates at room temperature about 300 K. To be able to detect small temperature variations, the cryogenic infrared detector is hermetically enclosed in a chamber, namely dewar, where the temperature is

* Corresponding author at: Changchun Institute of Optics, Fine Mechanics and Physics, Chinese Academy of Sciences, Changchun, Jilin 130033, China.
E-mail address: tian7jie@163.com (Q. Tian).

http://dx.doi.org/10.1016/j.infrared.2017.05.013
1350-4495/

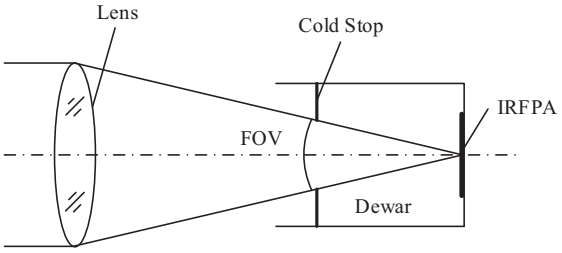

Fig. 1. Schematic diagram of F-number matching.

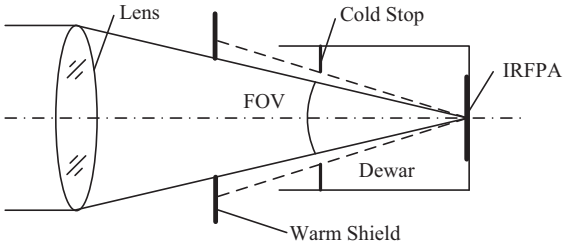

Fig. 2. Schematic diagram of using a warm shield.

kept constant (i.e., 77 K). Therefore, the flat warm shield, which operates at room temperature, is a high-temperature stray radiation source for the cryogenic infrared detector. The self-radiation of flat warm shield will certainly degrade the image quality. In order to weaken the self-radiation of flat warm shield, additional refrigeration equipment is required. However, those equipments will add extra weight and consume high cost. Another way to weaken the self-radiation of flat warm shield is to polish its surface. Whereas, the self-radiation of the system, namely the stray radiation, can be reflected by the polished surface and reach the IRFPA directly which will degrade the image quality as well. Consequently, no matter how the surface of flat warm shield is treated, it cannot suppress stray radiation efficiently while achieving F-number matching. To overcome the restriction, a spherical warm shield is required to achieve the F-number matching with the stray radiation being suppressed significantly. However, to our best knowledge, the details with regard to the spherical warm shield design have not been reported in any articles.

In this paper, we have introduced the detailed theory of spherical warm shield design for infrared imaging systems. A short outline of this paper is presented as follow: on the basis of the principle that stray radiation cannot directly reach the IRFPA, the theory of spherical warm shield design is deduced in detail in Section 2. Following this, a polished spherical warm shield, whose radius is 18 mm, is designed to turn the F-number of an F/2 cooled infrared detector to F/4. In Section 3, the stray radiation suppression performance and the alignment error of the designed spherical warm shield are analyzed by simulation. A comparison experiment is conducted in a chamber with controllable inside temperatures to evaluate the performance of the designed spherical warm shield in Section 4. It is concluded in Section 5 that the designed spherical warm shield cannot only achieve F-number matching but suppress stray radiation significantly. What's more, the theory of spherical warm shield design developed in this article is valid and can be employed by any infrared imaging systems.

2. Design of spherical warm shield

2.1. Determination of critical rays

The fundamental principle of the spherical warm shield design is to prevent the stray radiation from directly reaching the IRFPA. According to the reversibility principle of ray path, this principle means all the rays traced from the IRFPA are completely reflected back to the cryogenic dewar by the spherical warm shield. Meanwhile, the reflecting surface of spherical warm shield is polished and coated with high-reflection film, which has extraordinarily low emissivity compared with other structures.

The pertinent parameters required for the design of spherical warm shield are shown in Fig. 3. The X axis denotes the optical axis and the IRFPA is located at the point O(0,0), which is the origin of coordinate. The radius and height of the spherical warm shield are denoted as R and H, respectively. D is the diameter of the central hole of spherical warm shield; L denotes the distance from the central hole to the IRFPA; $O_i(x_i, 0)$ is the coordinate of the center of spherical warm shield; l denotes the length of the cryogenic dewar; b is the semi-diameter of the entrance pupil of detector and a denotes the half length of detector diagonal line.

The aim is to obtain the radius R and the height H of the spherical warm shield. Because of the rotational symmetry of optical systems, only the detector diagonal line is considered during the whole analysis process. Furthermore, we only need to analyze the rays propagating to the $-y$ direction, and the rays propagating to the $+y$ direction are the same due to the axial symmetry of detector diagonal line. As shown in Fig. 3, for the right triangle ΔO_i-EA_1, Eq. (1) should be satisfied

$$R = \sqrt{(L - x_i)^2 + (D/2)^2}. \tag{1}$$

And the quadratic equation of spherical warm shield is given by

$$\left[x - \left(L - \sqrt{R^2 - (D/2)^2}\right)\right]^2 + y^2 = R^2. \tag{2}$$

In order to make sure that all the rays traced from the IRFPA are completely reflected back to dewar, we need to determine the critical rays which can be used to calculate the radius range. As we can see from Fig. 3, the entrance pupil of detector restricts the FOV of the IRFPA. For a given pixel on the IRFPA, we define the ray that determines its FOV in $-y$ direction as the marginal ray. If the marginal rays are reflected back to dewar, other rays between the marginal rays will be reflected back as well. Therefore, it is essential to analyze the most outside marginal rays that pass through the rim of entrance pupil, namely the point $C(l, d)$ and $B(l, -d)$.

Considering the marginal rays passing through the edge point C (l, d) in Fig. 4, the boundary is determined by the point P and P_0, which are the intersection points between the most outside marginal rays and spherical warm shield. Assuming an arbitrary marginal ray intersecting at P_C on the spherical warm shield, in order to make it reflected back to dewar, the maximum angle of reflection must be less than $\angle O_i P_C B$, which is half of $\angle CP_C B$. Furthermore, with P_C moving from P to P_0, $\angle CP_C B$ is decreasing, which means the

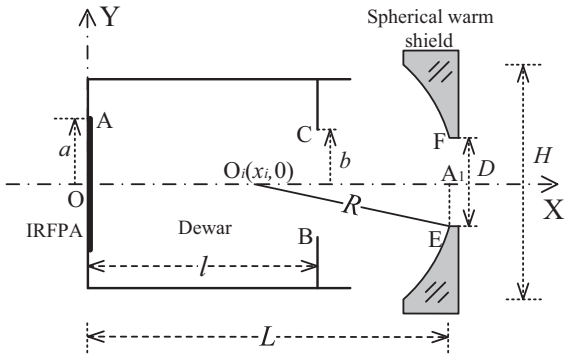

Fig. 3. Optical layout defining parameters of spherical warm shield.

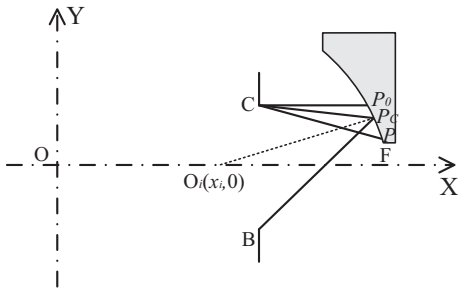

Fig. 4. Simplified schematic of marginal rays passing through edge point *C*.

maximum angle of reflection is determined by *P*, namely the marginal ray passing through point *C* and hitting on spherical warm shield at the maximum angle of incidence. In other word, if ray *CP* is reflected back to dewar, other marginal rays with smaller incident angles will be reflected as well. Thereupon, ray *CP* is the critical ray.

Fig. 5 exhibits the marginal rays passing through point $B(l, -d)$. The boundary is determined by point *Q* and Q_0, namely the intersection points between the most outside marginal rays and spherical warm shield. Assuming an arbitrary marginal ray intersecting at Q_B on the spherical warm shield, in order to make it reflected back to dewar, the critical condition is that the reflected ray reverses back as the same way it propagates outward or passes through the edge point $C(l, d)$. If the reflected ray reverses back as the way it propagates outward, the center of spherical warm shield locates at the intersection point of ray BQ_B and the *X* axis, namely the zero point of ray BQ_B. With the movement of point Q_B from Q_0 to *Q*, the zero point of ray BQ_B is increasing, which means the radius value is decreasing inversely according to Eq. (1). The critical condition is determined by point *Q*, namely the intersection point of spherical warm shield and the most outside marginal ray passing through point *B* at the maximum angle. Thereupon, the ray *BQ* is the critical ray. Besides, when point Q_B moves from Q_0 to *Q*, $\angle BQ_BC$ is decreasing, which means the maximum angle of incidence is determined by ray BQ_0. However, due to the axial symmetry we can learn that $\angle BQ_0C$ is less than $\angle CPB$ in Fig. 4, which means ray *CP* in Fig. 4 is the critical ray rather than ray BQ_0.

On the basis of the analysis presented above, we can learn that the radius range in Fig. 3 is determined by the critical ray *AB* and the critical ray *AC*, namely the marginal rays passing through the edge point of entrance pupil at the maximum angle. Moreover, the minimum height, which should cover the most outside marginal ray, is determined by the critical ray *AB* as well. For now we have determined the critical rays, and we are supposed to calculate the radius range.

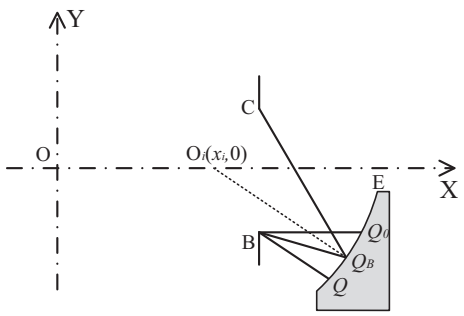

Fig. 5. Simplified schematic of marginal rays passing through edge point *B*.

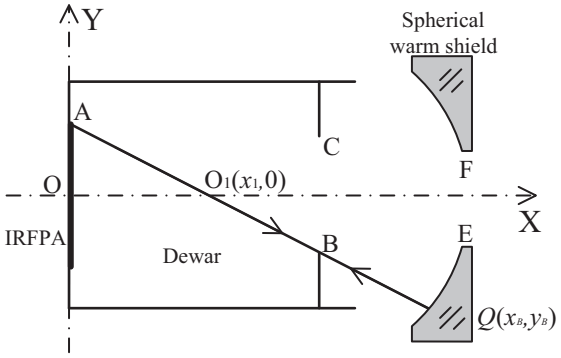

Fig. 6. Optical layout of the critical ray *AB*.

2.2. Geometry design

The critical ray *AB* originates from the positive edge of the detector diagonal line and passes at the negative edge of the entrance pupil. It strikes at $Q(x_B, y_B)$ on the reflecting surface and after reflection it goes back as the same way it propagates outwards, as shown in Fig. 6. The critical ray *AB* can be expressed as

$$y = k_1 \cdot x + b_1, \tag{3}$$

where $k_1 = -(a + b)/l$ and $b_1 = a$.According to the law of reflection, the center of spherical warm shield is located at the intersection point of the critical ray *AB* and the optical axis, namely the zero point of Eq. (3). The maximum radius is denoted by R_{max} and can be obtained by Eqs. (1) and (3). The minimum height of spherical warm shield, denoted by H_{min}, equals to $|2y_B|$ and can be obtained by substituting Eq. (3) into Eq. (2).

The critical ray *AC* originates from the positive edge of the detector diagonal line and goes through the positive edge of the entrance pupil. It intersects at $P(x_C, y_C)$ on the reflecting surface and after reflection it passes through the negative edge of the entrance pupil, as shown in Fig. 7. The critical ray *AC* can be written in the form of straight line equation as

$$y = k_2 \cdot x + b_2, \tag{4}$$

where $k_2 = (b - a)/l$ and $b_2 = a$.

And the reflected ray *PB* can be written in the linear form as

$$y = k_3 \cdot x + b_3, \tag{5}$$

where $k_3 = (y_C + b)/(x_C - l)$ and $b_3 = -l \cdot (y_C + b)/(x_C - l) - b$.

The point of spherical warm shield is assumed to locate at point $O_2(x_2, 0)$, which can be acquired by

$$\frac{|k_3 \cdot x_2 + b_3|}{\sqrt{k_3^2 + 1}} = \frac{|k_2 \cdot x_2 + b_2|}{\sqrt{k_2^2 + 1}}. \tag{6}$$

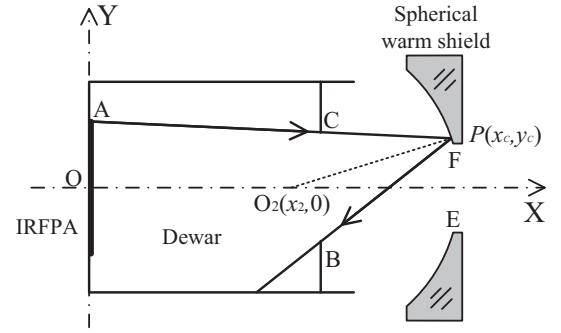

Fig. 7. Optical layout of the critical ray *AC*.

The minimum radius is denoted by R_{min} and can be obtained by submitting $O_2(x_2, 0)$ to Eq. (1).

For now we have acquired the parameter range of the spherical warm shield, which can be expressed as

$$\left.\begin{array}{l} R \leqslant R_{max} \\ R \geqslant R_{min} \\ H \geqslant H_{min} \end{array}\right\}. \tag{7}$$

As shown in Fig. 3, the distance between the central hole of spherical warm shield and the IRFPA is L. In practical applications, the distance L should be chosen appropriately considering actual situations, not too large or too small. Theoretically, the stray radiation cannot directly reach the IRFPA as long as Eq. (7) is satisfied. Moreover, since the spherical warm shield is polished and covered with high-reflection film, its self-radiation is at extremely low level. Consequently, apart from the ability to achieve F-number matching, the spherical warm shield is able to improve the stray radiation suppression performance of an infrared imaging system.

2.3. Numerical example

To verify the design theory developed above, we design a spherical warm shield to match an F/4 system with an F/2 infrared detector. The pertinent parameters required to design the spherical warm shield are presented as follows. For our cryogenic infrared detector, the length of detector diagonal line is 12.294 mm, which means a equals to 6.147 mm. The entrance pupil of the detector is 10 mm, which means b is equivalent to 5 mm and l equals to 20 mm. For typical infrared imaging systems, the distance between the IRFPA and the last surface of optics is in the range [27 mm, 35 mm]. If the distance is too small, the optics are hard to assemble. If the distance is too large, the stray radiation from mechanical structures between the IRFPA and the last surface of optics is easy to be scattered and reaches the IRFPA directly. Hence, the range [27 mm, 35 mm] is adoptable for typical infrared imaging systems in practical applications. Of course, if there are some special infrared imaging systems, the distance must be chosen according to actual conditions.

In order to ensure that the spherical warm shield is easy to fabricate and assemble in practical applications, we recommend to choose the radius R and distance L as integers. For all the integers in range [27 mm, 35 mm], only 28 mm and 32 mm can be divisible by 4. Considering the thickness of the spherical warm shield, 28 mm is too small to locate the spherical warm shield. Consequently, we decide to put the spherical warm shield at the position where it is 32 mm away from the IRFPA, which means L equals to 32 mm and the diameter of central hole, namely D, is 8 mm.

In summary, the pertinent parameters required for the design of spherical warm shield can be concluded as follows:

$$\left.\begin{array}{l} D = 8 \\ L = 32 \\ a = 6.147 \\ b = 5 \\ l = 20 \end{array}\right\}. \tag{8}$$

On the basis of the design process introduced above, we can acquire the parameter range of spherical warm shield. According to Eq. (3), we can learn that the intersection point of critical ray AB and the optical axis, namely the zero point of Eq. (3), is 11.029, which means x_1 is equivalent to 11.029. Submitting $O_1(11.029, 0)$ into Eq. (1), we can obtain the maximum radius is 21.349 mm, which means R_{max} equals to 21.349 mm. Similarly, submitting permanent parameters into Eqs. from (4)–(6), we can acquire that x_2 equals to 18.151. Substituting $O_2(18.151, 0)$ into Eq. (1) yields that the minimum radius, namely R_{min}, is equivalent to 14.415 mm. For now, we have got the radius range, which can be expressed as [14.415 mm, 21.349 mm].

In practical applications, the distance between the IRFPA and the central hole of spherical warm shield is not exactly 32 mm due to the alignment error. In order to make the spherical warm shield easy to be fabricated, we suggest to choose the radius value as an integer. Besides, if we choose the critical value in range [14.415 mm, 21.349 mm], such as 15 mm or 21 mm, the alignment error may make the selected radius out of the valid range. So we recommend to choose the median value in range [14.415 mm, 21.349 mm] considering the alignment error. Submitting R = 18 mm into Eq. (2) yields the minimum height is 21.152 mm. Similarly, we select 25 mm as the height considering the alignment error and the fabrication simplicity. In conclusion, the location and dimension of the designed spherical warm shield can be summarized as follows:

$$\left.\begin{array}{l} D = 8 \text{ mm} \\ L = 32 \text{ mm} \\ R = 18 \text{ mm} \\ H = 25 \text{ mm} \end{array}\right\}. \tag{9}$$

3. Performance evaluation by simulation

3.1. Simulation of stray radiation suppression performance

Before fabricating the spherical warm shield designed above, we are supposed to analysis its performance and the influence of alignment error on it by simulation.

The analysis model of the spherical warm shield designed above is established. Additionally, there are two flat warm shields, which have same parameters and are treated in two ways, as a comparison. One is painted black, and the other is polished. Both of the spherical and flat warm shield analysis models are displayed in Fig. 8. The stray radiation sources can be classified into two categories. One is the self-radiation of warm shield, and the other is the radiation from the uncooled part of detector and the mechanical structures. Both of the stray radiation have been considered in Fig. 8 and the white dots represent the stray radiation source positions. The F-number of the detector has been changed from F/2 to F/4 owing to the addition of warm shield. We treat the spherical warm shield as a mirror surface with a reflectivity of 0.9 and an emissivity of 0.1. As for the flat warm shield, the emissivity of the black-painted one is set to 0.9, and the reflectivity equals to 0.1. The emissivity of the polished one is set to 0.1, and the reflectivity is equivalent to 0.9. Both of the analysis models are assumed to be at the ambient temperature 20 °C. Previous simulation has illustrated that when the number of traced rays is larger than 24,000,000,000, the simulation results tend to be stable. Consequently, in order to ensure the convergence of the simulation results, the number of traced rays is set to 30,000,000,000.

After the ray tracing, we get the average irradiance caused by the spherical warm shield is 1.0771×10^{-8}W·mm^{-2}. As an apparent contrast, the average irradiance caused by the black-painted and the polished flat warm shield reaches about 1.2378×10^{-7}W·mm^{-2} and 1.1695×10^{-7}W·mm^{-2}, respectively. In other word, the irradiance caused by the flat warm shields is over ten times than the irradiance caused by the spherical warm shield. More importantly, there is no stray radiation that can directly reach the IRFPA except for the self-radiation of the spherical warm shield, which is extremely low. Consequently, we can draw the conclusion that apart from the capability of achieving F-number matching, the spherical warm shield has an overwhelming performance than the flat warm shield in terms of improving the stray radiation suppression performance of infrared imaging systems.

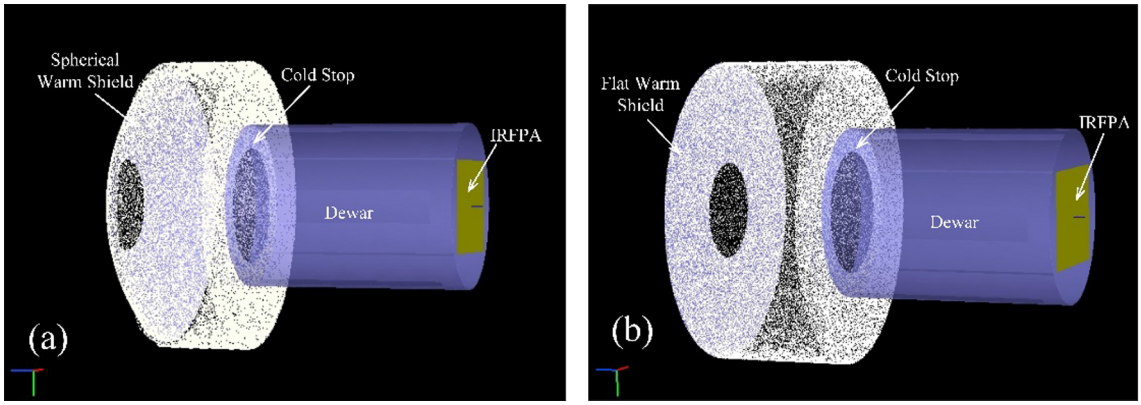

Fig. 8. Analysis models. (a) The analysis model of the spherical warm shield. (b) The analysis model of the flat warm shield. What should be noted is that only 120,000 stray radiation source positions are drawn for both of the models.

3.2. Simulation of alignment error

In spite of the fact that the simulation results have demonstrated that the spherical warm shield designed above can be used to achieve F-number matching, there will be some distance and eccentric deviations namely alignment errors in practical applications which should be analyzed as well.

According to current alignment accuracy, the distance and eccentric deviations can be restricted within ±0.5 mm. Hence, we analyze the spherical warm shield with different distance errors varying from −0.5 mm to 0.5 mm with 0.1 mm as the interval. Similarly, the eccentric error is set to varying from −0.5 mm to 0.5 mm with the interval of 0.1 mm. The ray tracing results are presented in Fig. 9.

As illustrated in Fig. 9, the maximum relative errors caused by the distance deviation and the eccentric deviation reach only 1.11% and 0.0611% respectively, which are acceptable in practical applications. More importantly, even though there are some alignment errors, there is still no stray radiation that can directly reach the IRFPA in addition to the self-radiation of spherical warm shield which is extraordinarily low. In other words, the spherical warm shield designed above is not sensitive to alignment errors and can be used in practical applications.

In summary, the simulation results have demonstrated that the spherical warm shield designed above can not only achieve F-number matching but have a prominent performance in the field of stray radiation suppression, with the advantage of not sensitive to alignment errors.

4. Radiometric calibration experiments and results

4.1. Experimental setup

The theoretical analysis and simulation results have demonstrated that the spherical warm shield designed above can be used to match optics with the detector and to suppress stray radiation. To further evaluate the performance of the designed spherical warm shield experimentally, the spherical warm shield is fabricated. Meanwhile, both of the two flat warm shields analyzed above are fabricated as well for comparison. The photo of warm shields is shown in Fig. 10. The parameters of the designed spherical warm shield are depicted in detail in Fig. 11.

The reflecting surface of the spherical warm shield is polished and covered with aluminum coating with an average reflectivity of 0.93 across the spectral band from 3.7 μm to 4.8 μm. The RMS surface micro-roughness of the reflecting surface is less than λ/30 (λ = 0.6328 μm). As a contrast, one of the flat warm shields is painted black with an emissivity of about 0.9. The other is polished and the reflectivity is about 0.9.

In order to obtain the response and offset of the infrared detector, the radiometric calibration must be carried out. In this paper, the near-extended-source method is adopted to achieve the radio-

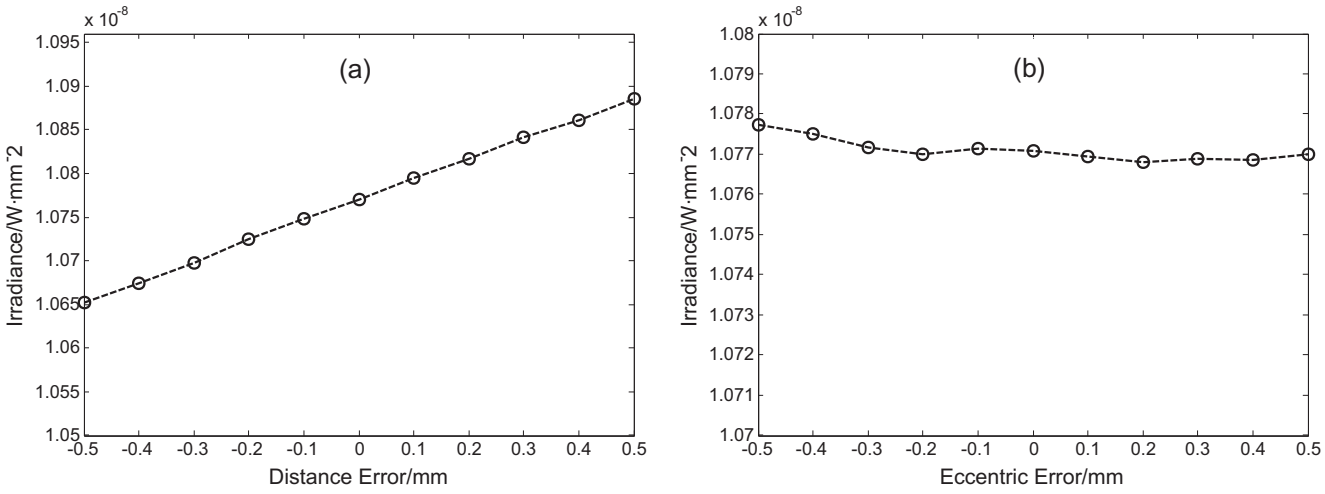

Fig. 9. (a) Average irradiance caused by spherical warm shield with different distance errors. (b) Average irradiance caused by spherical warm shield with different eccentric errors.

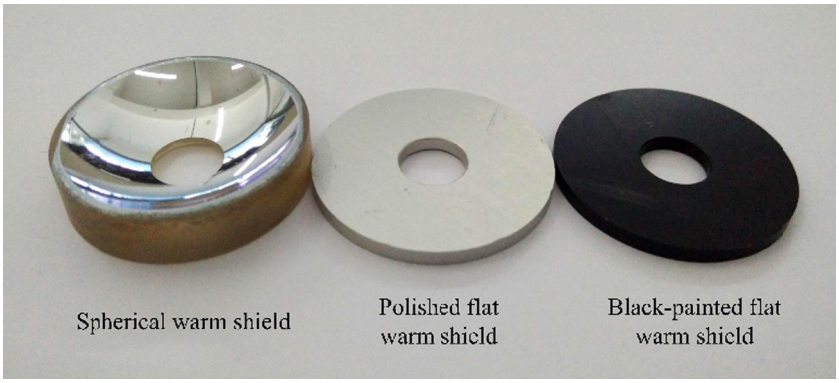

Fig. 10. Photo of warm shields.

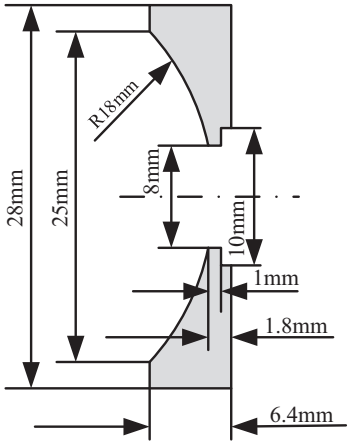

Fig. 11. Parameter of the designed spherical warm shield.

metric calibration. Generally, the reference source, namely the blackbody, is positioned closely to optics so as to remove the atmospheric effect. The relation between the detector output gray value (Digital Number, DN) and the incident radiance of blackbody is linear within the linear response range of a cooled infrared detector, and can be expressed as [7,8]

$$h = G \cdot L + B = G \cdot L + h_{warm} + h_{det}, \tag{10}$$

where h is the output gray value of detector, G is the radiance response, B denotes the offset of radiometric calibration resulting from the radiation caused by warm shield and reaches the IRFPA and the internal factors of infrared detector. For a given cooled infrared detector, the response G and the internal factors h_{det} will not vary at a preselected integration time [9]. But the detector output caused by the warm shield h_{warm} will change with the ambient temperature variation. Therefore, the effect of different warm shields can be embodied by the output gray value of the infrared detector.

The experiments were conducted in a chamber with controllable and stable inside temperatures to ensure good performance. Experiments have suggested that the temperature accuracy inside the chamber is ±0.5 °C. The SR-800R-A extended-area blackbody of CI systems, which is chosen as the reference source, has a size of 100 mm × 100 mm, and exhibits an effective emissivity of about 0.97 over the waveband from 3.7 μm to 4.8 μm. The temperature accuracy of the selected blackbody is ±0.01 °C over the temperature range from 0 °C to 125 °C. The cooled mid-wave infrared (MWIR) detector of forward looking infrared (FLIR) systems works in 3.7 μm–4.8 μm waveband with an F-number of F/2. And the detector has a focal plane array of 320 × 256 pixels, with a 14 bit digital output. The experimental setup is sketched in Fig. 12.

The experiments were carried out in three steps:

(1) The cooled MWIR detector was calibrated to obtain the detector internal factors, namely h_{det}, as the standard values under the ambient temperature varying from 10 °C to 50 °C with 10 °C as the interval.
(2) Considering the effect of the thickness of dewar window, the spherical warm shield was placed at the position where it is 6.7 mm away from the dewar window. Then the radiometric calibration was performed under the same ambient temperature with the same interval.
(3) The spherical warm shield was replaced by the flat warm shield, and the same procedure presented in step (2) was repeated.

4.2. Results and analysis

The F-number of the F/2 infrared detector has been turned to F/4, due to the addition of the warm shield. The offset of the infra-

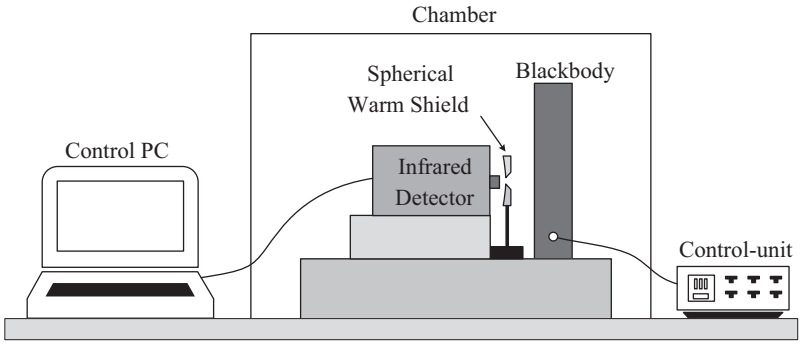

Fig. 12. The experimental setup for radiometric calibration.

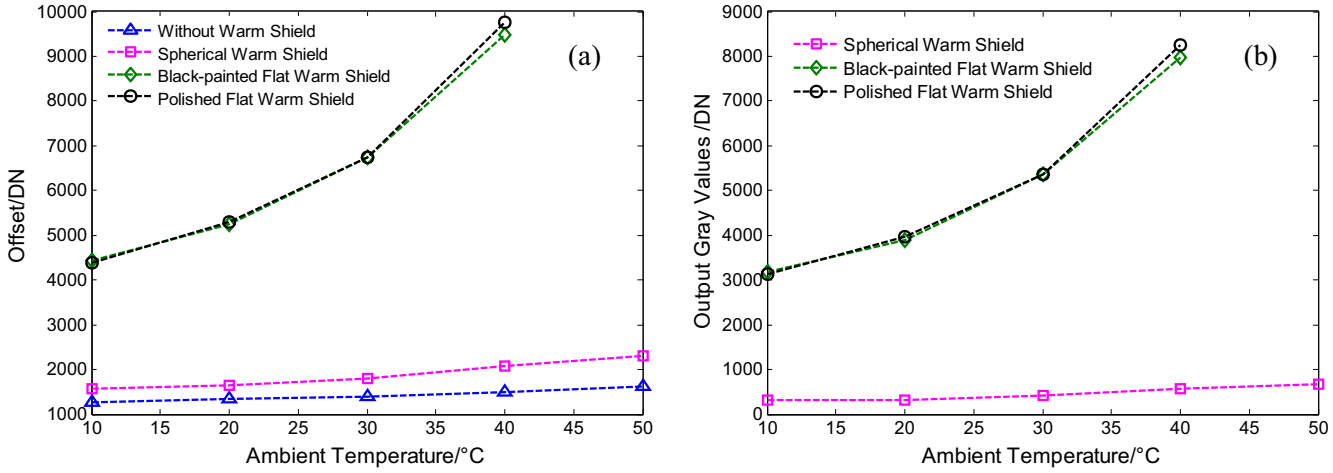

Fig. 13. (a) The offset of detector with different warm shields. (b) The output gray value caused by different warm shields.

red detector with different warm shields is presented in Fig. 13(a). It is obviously illustrated in Fig. 13(a) that the offset of radiometric calibration increases when the ambient temperature rises. Furthermore, the output gray value, caused by different warm shields, is calculated and shown in Fig. 13(b). As we can see from Fig. 13(b), the detector output induced by the two flat warm shields increases rapidly with the ambient temperature rising. As an apparent contrast, the output gray value induced by spherical warm shield just increases slowly and slightly. More specifically, the output gray value caused by the two flat warm shields is over ten times than the output gray value caused by spherical warm shield under the same ambient temperature. The reason lies in the fact that the spherical warm shield cannot only prevent stray radiation from directly reaching the IRFPA but have an extremely low level of self-radiation. Nevertheless, the two flat warm shields have neither of the advantages. Besides, the output gray value caused by the two differently treated flat warm shields is nearly equivalent, which is similar to the analysis results. The experimental results are in agreement with the simulation analysis results in Section 3, which demonstrates that the simulation analysis in Section 3 is valid. The experimental and simulation results have illustrated that no matter how the surface of flat warm shield is treated, the flat warm shield cannot suppress stray radiation. One point should be noted that when the ambient temperature is 50 °C, the MWIR detector with flat warm shield has been saturated, which means the detector is out of use. Hence, we can draw the conclusion that the infrared detector with spherical warm shield has higher dynamic range.

In summary, on the basis of the experimental results presented above, we can conclude that the spherical warm shield has an outstanding performance in the field of suppressing stray radiation of infrared imaging systems, in addition to the capability of achieving F-number matching. Furthermore, the theory of spherical warm shield design developed in this paper is valid and can be employed by any infrared imaging systems. Although the spherical warm shield can suppress stray radiation sufficiently, it doesn't mean the optical designer can design the optics at will. One point should be noted that the optical designer should take the spherical warm shield as the aperture stop in order to suppress stray radiation significantly.

5. Conclusions

To achieve exact F-number matching, overcome the restriction from the fixed F-number of infrared detector and suppress stray radiation simultaneously, the detailed theory of spherical warm shield design has been introduced on the basis of the principle that stray radiation cannot directly reach the IRFPA. According to the theory developed above, a polished spherical warm shield, whose radius is 18 mm, has been designed to turn the F-number of an F/2 infrared detector to F/4. The stray radiation suppression performance and the alignment error of the designed spherical warm shield have been analyzed by simulation. And simulation results indicate that the designed spherical warm shield can sufficiently suppress stray radiation with the advantage of not sensitive to alignment errors. Finally, a contrast radiometric calibration experiment, between the designed spherical warm shield and two flat warm shields with different surface characteristics, is performed in a chamber with controllable inside temperatures. And the experimental results show that the output gray value caused by the spherical warm shield is less than one-tenth of the output gray value caused by the flat warm shield under the same ambient temperature. The reason lies in the fact that the spherical warm shield cannot only prevent stray radiation from directly reaching the IRFPA but have an extremely low level of self-radiation. Therefore, in addition to the capability of achieve F-number matching, the spherical warm shield can suppress the stray radiation sufficiently. What's more, the theory of spherical warm shield design developed in the paper is valid, and can be adopted by arbitrary infrared imaging systems.

The main benefits of using a spherical warm shield are presented as follows:

- The F-number of infrared imaging systems is no longer restricted by the F-number of infrared detectors.
- The stray radiation of infrared imaging system can be suppressed sufficiently.
- There is no need for the refrigeration equipment, so the cost, size and weight can be reduced.

Conflict of interest

The authors declare that there is no conflict of interest.

References

[1] Y. Zhu, X. Zhang, T. Liu, Y.X. Wu, G.W. Shi, L.J. Wang, Internal and external stray radiation suppression for LWIR catadioptric telescope using non-sequential ray tracing, Infrared Phys. Technol. 71 (2015) 163–170.
[2] A.V. Pravdivtsev, M.N. Akram, Simulation and assessment of stray light effects in infrared cameras using non-sequential ray tracing, Infrared Phys. Technol. 60 (2013) 306–311.
[3] E. Fest, Stray Light Analysis and Control, 2013.

[4] M.N. Akram, Design of a multiple-field-of-view optical system for 3 to 5μm infrared focal-plane arrays, Opt. Eng. 42 (2003) 1704–1714.
[5] A. Deslis, Optical design of a warm shield for the 8 to 12-micron wavelength region, Proc. SPIE 6288 (2006) 628803.
[6] N. Gat, J.Y. Zhang, M.D. Li, L. Chen, H. Gurrola, Variable cold stop for matching IR cameras to multiple F-number optics, Proc. SPIE 6542 (2007) 65420Y.
[7] Z.Y. Sun, S.T. Chang, W. Zhu, Radiometric calibration method for large aperture infrared system with broad dynamic range, Appl. Opt. 54 (2015) 4659–4666.
[8] S.T. Chang, Y.Y. Zhang, Z.Y. Sun, M. Li, Method to remove the effect of ambient temperature on radiometric calibration, Appl. Opt. 53 (2014) 6274–6279.
[9] Y. Lü, X. He, Z.H. Wei, Z.Y. Sun, S.T. Chang, Ambient temperature-independent dual-band mid-infrared radiation thermometry, Appl. Opt. 55 (2016) 2169–2174.